Annals of Nuclear Energy 89 (2016) 63–69

Contents lists available at ScienceDirect

Annals of Nuclear Energy

journal homepage: www.elsevier.com/locate/anucene

# Shielding properties of protective thin film coatings and blended concrete compositions for high level waste storage packages

Michael A. Fusco [a,*], Leigh Winfrey [b], Mohamed A. Bourham [a]

[a] North Carolina State University, Department of Nuclear Engineering, Raleigh, NC 27695-7909, USA
[b] University of Florida, Nuclear Engineering Program, Department of Materials Science and Engineering, Gainesville, FL 32611-6400, USA

ARTICLE INFO

*Article history:*
Received 10 September 2015
Received in revised form 20 November 2015
Accepted 23 November 2015
Available online 30 November 2015

*Keywords:*
Shielding
Protective coatings
High-level waste storage
Dry cask overpack composition
Concrete blending
Gamma ray shielding

ABSTRACT

Various thin film coatings have been proposed to protect stainless steel high level waste (HLW) containers from premature failure due to localized corrosion, hydrogen embrittlement, and mechanical wear. These coatings include TiN, $ZrO_2$, $MoS_2$, $TiO_2$, and $Al_2O_3$, to be deposited either in multiple layers or as a thicker, single-layer composite. Linear attenuation coefficients of these materials have been simulated using MicroShield and measured experimentally for various photon energies. Additionally, spent fuel casks with overpacks made of two different types of concrete were simulated to compare exposure rate at the cask surface. In the energy range that is significant for high level waste storage all coating materials possess very similar attenuation behavior. A specialty concrete, containing magnetite ($Fe_3O_4$) and lead oxide (PbO), reduces the exposure rate at the outer surface of the overpack by several orders of magnitude. The higher-Z elements not present in ordinary concrete greatly increase attenuation of intermediate-energy gammas (0.4–1.0 MeV). The thin film coatings do not affect the shielding capabilities of the HLW packaging, as their total proposed thickness is nearly three orders of magnitude less than the mean free path (MFP) of the primary photons of interest.

© 2015 Elsevier Ltd. All rights reserved.

## 1. Introduction

Storage of spent nuclear fuel from commercial reactors and government-controlled high level waste (HLW) is one of the most important issues facing the nuclear industry. On-site dry cask storage is the only current long term storage option for commercial spent fuel, and thus, limiting exposure outside of the cask is of high priority. Dry storage casks consist primarily of a steel canister and concrete overpack, often with a glass layer in between (Bare and Torgerson, 2001). HLW canisters are typically made of stainless steel because of its good mechanical strength and corrosion resistance (Yim and Murty, 2000; Farmer et al., 2003; Lambert et al., 2012). However, stainless steel suffers from intergranular corrosion due to carbide buildup at grain boundaries and stress corrosion cracking (SCC) due to residual stresses from welding in the presence of chloride ions (Revie and Uhlig, 2008). Additionally, mechanical wear and embrittlement from hydrogen diffusion pose a threat to the long term integrity of spent fuel canisters. A lack of in situ monitoring coupled with the relative unpredictability of localized corrosion and embrittlement from gas diffusion makes canister lifetime difficult to predict. The US NRC mandates that high level waste containers must remain intact for 300–1000 years (U.S. Nuclear Regulatory Commission, 2002), making materials research for HLW storage imperative.

In order to combat premature failure of stainless steel canisters, various thin-film coatings have been proposed (Winfrey and Bourham, 2013). These coatings include titanium nitride (TiN), molybdenum disulfide ($MoS_2$), and Zirconia ($ZrO_2$), titania ($TiO_2$), and alumina ($Al_2O_3$) as an eventual composite, and have been shown to be good barriers to localized corrosion, hydrogen diffusion, and mechanical wear (Checchetto et al., 1996; Scheffing et al., 2006).

The middle coating layer is a composite of the three oxides, and is commonly referred to as Zirconolite.

If these coatings are to be utilized to protect HLW containers, their attenuation properties must be known. Mass attenuation coefficients provide an adequate measure of the shielding capabilities of each material. The mass attenuation coefficient is independent of density, allowing for direct comparison between materials. A simulation study on the heavy particle impact on such multi-layered coatings, as in Fig. 1, has shown that 2 MeV particles can cause damage in the first 10 μm of the TiN layer if neutrons leak through cracks and reach the coatings (Radwan et al., 2015).

* Corresponding author.
*E-mail addresses:* mfusco@ncsu.edu (M.A. Fusco), winfrey@mse.ufl.edu (L. Winfrey), bourham@ncsu.edu (M.A. Bourham).

http://dx.doi.org/10.1016/j.anucene.2015.11.026
0306-4549/© 2015 Elsevier Ltd. All rights reserved.

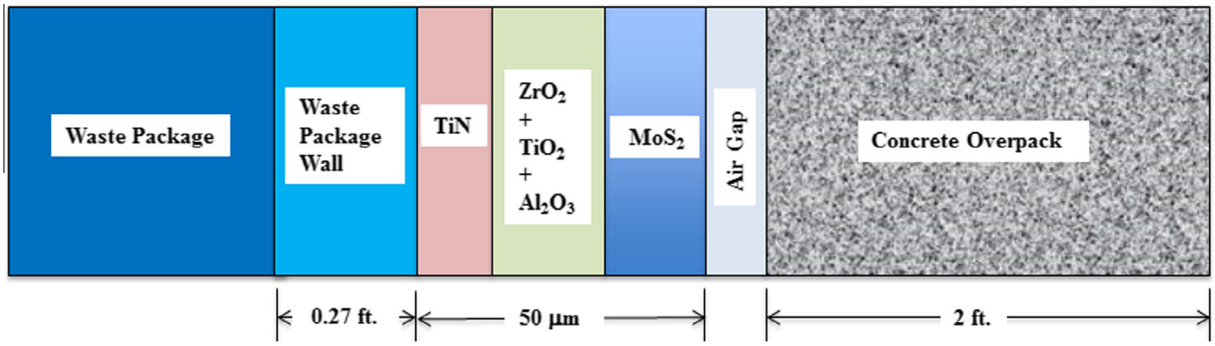


**Fig. 1.** Multilayer coatings for high level waste storage (not to scale).

Recently there has been interest in specialty concrete for radiation shielding applications. The composition of concrete can be modified using additives and different forms of aggregates, making it an ideal material to be tailored toward specific uses. A computational study on various compositions of concrete for gamma attenuation, has shown that adding magnetite ($Fe_3O_4$) and lead oxide (PbO) in specific concentrations to standard concrete increases attenuation and greatly reduces exposure rate outside the spent fuel cask (Waly and Bourham, 2015), and a specific concrete mixture, referred to as 'concrete-6' in their paper will be used as a comparison to ordinary concrete in the present study.

## 2. Methods

### 2.1. Computational methods

Linear attenuation coefficients are calculated using MicroShield 9.05 (GrooveSoftware, 2012). The mass attenuation coefficient is calculated from the linear attenuation coefficient divided by the mass density of the absorber material and is given by the exponential attenuation law:

$$\frac{\mu}{\rho} = \frac{-1}{\rho x} \ln\left(\frac{I}{I_0}\right) \quad (1)$$

where $\mu$ is the linear attenuation coefficient ($cm^{-1}$), $\rho$ is mass density ($g/cm^3$), $\mu/\rho$ is the mass attenuation coefficient ($cm^2/g$), $x$ is the absorber thickness (cm), $I_0$ is the initial photon intensity, and $I$ is the transmitted photon intensity.

MicroShield computes the theoretical attenuation coefficient at desired photon energies using material composition and density. It has also been used to assess the exposure rate outside a typical spent fuel cask, as well as to assess the change in shielding effectiveness using multilayer protective coatings and magnetite/lead oxide-doped concrete "concrete 6" (Waly and Bourham, 2015). This concrete consists of 13.98% cement, 7.63% water, 23.5% aggregate (mainly $SiO_2$), 39.195% magnetite, and 15.678% lead oxide. The complete chemical composition of this proposed concrete mixture is given in Waly and Bourham (2015).

The cask utilized in this study consists of a cylindrical volume of spent fuel with a height of 20 ft. and 8.727-ft. radius. The steel canister is 0.27 ft. thick, and the concrete overpack is 2 ft. thick. Three coating layers are added to the outside of the steel canister, which combined are 50 µm thick. The radiation source used in the MicroShield simulations comes from Surry plant spent fuel depleted using ORIGEN at 38.6 GWd/MTU (Naegeli, 2004) and is given in Table 1. The photon activity by energy group is scaled to represent 16 MTU per storage cask. At 0.4–0.5 MTU per assembly in a typical PWR, this assumes between 32 and 40 assemblies per cask. This is conservative given that the NRC considers between 2 dozen and 6 dozen assemblies per cask depending on the type (U.S. Nuclear Regulatory Commission, 2015). The dose point is taken half way up the cask at the outer surface as illustrated in Fig. 2.

**Table 1**
Source specification for spent fuel cask simulation – 38.6 GWd/MTU Surry plant.

| Mean photon energy (MeV) | Activity/MTU (Photons/s) | % Energy activity |
|---|---|---|
| 0.015 | 3.08E+09 | 0.00000 |
| 0.02 | 7.03E+09 | 0.00000 |
| 0.03 | 1.55E+14 | 0.31680 |
| 0.04 | 4.67E+13 | 0.12730 |
| 0.05 | 2.82E+12 | 0.00960 |
| 0.06 | 4.61E+13 | 0.18850 |
| 0.08 | 2.38E+12 | 0.01300 |
| 0.10 | 2.22E+13 | 0.15130 |
| 0.15 | 1.59E+10 | 0.00020 |
| 0.20 | 3.74E+12 | 0.05100 |
| 0.30 | 4.39E+11 | 0.00900 |
| 0.40 | 7.19E+11 | 0.01960 |
| 0.50 | 6.34E+11 | 0.02160 |
| 0.60 | 2.32E+15 | 94.8505 |
| 0.80 | 2.25E+13 | 1.22650 |
| 1.00 | 1.53E+13 | 1.04250 |
| 1.50 | 1.93E+13 | 1.97260 |
| 2.00 | 2.91E+06 | 0.00000 |
| Total | 2.66E+15 | |

The source specification for spent fuel cask simulation shows that the 0.6 MeV photon energy group contributes almost 95% of the energy activity, mostly from the decay of Cs-137. Also of interest are three higher energy groups: 0.8, 1.0, and 1.5 MeV, which have fairly high activity and are more difficult to shield than the lower energy gammas. These will likely contribute much of the total exposure rate. There are several energy groups in the tens of keV range that have high activity, but they are quite easily shielded and will not contribute significantly to exposure.

### 2.2. Experimental methods

In order to corroborate theoretical calculations using the MicroShield code, gamma attenuation experiments have been performed. The radiation sources are 1" disks of Ba-133, Cs-137, and Co-60 to determine attenuation coefficients at four photon energies: 356 keV, 661.7 keV, 1173 keV, and 1332.5 keV, respectively. The detector is a $2'' \times 2''$ sodium iodide (NaI) scintillator, with built-in photomultiplier tube (PMT) and preamplifier, connected to a high voltage power supply, shaping amplifier, and multichannel analyzer (MCA). The three gamma sources are tested separately to avoid self-shielding. The detector is placed 60 cm directly above the source, and the disks are placed one-third of the way between source and detector, assuring most photons reaching the detector pass through the disk. Fig. 3 illustrates the experimental set up for gamma attenuation measurements.

Download English Version:

https://daneshyari.com/en/article/1728054

Download Persian Version:

https://daneshyari.com/article/1728054

Daneshyari.com